THE JOURNAL OF BIOLOGICAL CHEMISTRY
Vol. 279, No. 1, Issue of January 2, pp. 19–25, 2004

Printed in U.S.A.

TRPM6 Forms the Mg^{2+} Influx Channel Involved in Intestinal and Renal Mg^{2+} Absorption*

Received for publication, October 13, 2003, and in revised form, October 22, 2003
Published, JBC Papers in Press, October 23, 2003, DOI 10.1074/jbc.M311201200

Thomas Voets‡§, Bernd Nilius‡, Susan Hoefs¶, Annemiete W. C. M. van der Kemp¶, Guy Droogmans‡, Rene J. M. Bindels¶, and Joost G. J. Hoenderop¶‖

From the ‡Department of Physiology, Campus Gasthuisberg, Katholieke Universiteit Leuven, B-3000 Leuven, Belgium and the ¶Department of Physiology, Nijmegen Center for Molecular Life Sciences, University Medical Center Nijmegen, NL-6500 HB Nijmegen, The Netherlands

Mg^{2+} is an essential ion involved in a multitude of physiological and biochemical processes and a major constituent of bone tissue. Mg^{2+} homeostasis in mammals depends on the equilibrium between intestinal Mg^{2+} absorption and renal Mg^{2+} excretion, but little is known about the molecular nature of the proteins involved in the transepithelial transport of Mg^{2+} in these organs. Recently, it was shown that patients with mutations in TRPM6, a member of the transient receptor potential family of cation channels, suffer from hypomagnesemia with secondary hypocalcemia (HSH) as a result of impaired renal and/or intestinal Mg^{2+} handling. Here, we show that TRPM6 is specifically localized along the apical membrane of the renal distal convoluted tubule and the brush-border membrane of the small intestine, epithelia particularly associated with active Mg^{2+} (re)absorption. In kidney, parvalbumin and calbindin-D_{28K}, two divalent-binding proteins, are coexpressed with TRPM6 and might function as intracellular Mg^{2+} buffers in the distal convoluted tubule. Heterologous expression of wild-type TRPM6 but not TRPM6 mutants identified in HSH patients induces a Mg^{2+}- and Ca^{2+}-permeable cation channel tightly regulated by intracellular Mg^{2+} levels. The TRPM6-induced channel displays strong outward rectification, has a 5-fold higher affinity for Mg^{2+} than for Ca^{2+}, and is blocked in a voltage-dependent manner by ruthenium red. Our data indicate that TRPM6 comprises all or part of the apical Mg^{2+} channel of Mg^{2+}-absorbing epithelia.

Mg^{2+} is the fourth most abundant cation in the body and the second most common cation in the intracellular fluid. Homeostasis of Mg^{2+} levels is tightly regulated and depends on the balance between intestinal absorption and renal excretion. The kidney provides the most sensitive control for the Mg^{2+} balance. About 80% of the total serum Mg^{2+} is ultrafiltered through the glomerular membrane and subsequently reabsorbed in consecutive segments of the nephron (1). The final urinary excretion of Mg^{2+} is mainly determined by the active reabsorption of Mg^{2+} in the distal convoluted tubule (DCT),[1] because virtually no reabsorption takes places beyond this segment (1).

Recently, a positional candidate screening approach in consanguineous families with hypomagnesemia with secondary hypocalcemia (HSH) revealed a critical region identified on chromosome 9q21.13 (2, 3). Individuals suffering from HSH display neurologic symptoms including seizures and tetany during infancy. These symptoms can be suppressed by life-long dietary magnesium supplementation, but, untreated, the disease may be fatal or result in neurological damage. The pathophysiology of HSH is largely unknown, but physiological studies have shown that there are defects in both intestinal Mg^{2+} absorption and renal Mg^{2+} reabsorption. Subsequent analysis of the critical region pointed to a gene, *TRPM6*, which was mutated in patients with HSH (2, 3). The TRPM6 protein is a member of the transient receptor potential channel (TRP) family (4).

Based on the structural and sequence similarities between individual TRP proteins, three subgroups are distinguished, namely the canonical TRPC-, the vanilloid-like TRPV-, and the melastatin-like TRPM subfamilies. Most members of the TRPC- and TRPV-subfamilies have been characterized as Ca^{2+}-permeable cation channels playing a role in Ca^{2+} homeostasis and signaling (4). However, the functional characterization of TRPM proteins is much more incomplete. TRPM6 shows 50% sequence homology with TRPM7 (also known as TRP-PLIK), which forms a Ca^{2+} and Mg^{2+}-permeable cation channel. Unlike other members of the TRP family, TRPM6 and TRPM7 contain long carboxyl-terminal domains with similarity to the α-kinases (5). The identification of *TRPM6* as the gene mutated in HSH represents the first case in which a human disorder has been attributed to a channel kinase.

The aim of the present study was to functionally characterize TRPM6 as the first molecularly identified protein involved in active Mg^{2+} (re)absorption. To this end, the (sub)localization of TRPM6 was investigated by immunohistochemical analysis of kidney and duodenum sections. Subsequently, human TRPM6 cDNA was cloned, transfected into human embryonic kidney

* This work was supported by Dutch Organization of Scientific Research Grant Zon-Mw 016.006.001, Dutch Kidney Foundation Grant C02.2030, and, in part, by the Belgian Federal Government, the Flemish Government, Onderzoeksraad Katholieke Universiteit Leuven Fund for Scientific Research Grants G.0214.99, G.0136.00, G.0118.00, and G.0172.03, and the Interuniversity Poles of Attraction Program (IUAP), Prime Ministers Office. The costs of publication of this article were defrayed in part by the payment of page charges. This article must therefore be hereby marked "*advertisement*" in accordance with 18 U.S.C. Section 1734 solely to indicate this fact.

§ Postdoctoral Fellow of the Fund for Scientific Research-Flanders (F.W.O.-Vlaanderen, Belgium) and to whom correspondence may be addressed. E-mail: Thomas.Voets@med.kuleuven.ac.be.

‖ To whom correspondence may be addressed: 160 Cell Physiology, University Medical Center Nijmegen, P. O. Box 9101, NL-6500 HB Nijmegen, The Netherlands. Tel.: 31-24-3610571; Fax: 31-24-3616413; E-mail: J.Hoenderop@ncmls.kun.nl.

[1] The abbreviations used are: DCT, distal convoluted tubule; DM-nitrophen, dimethoxynitrophenamine tetrasodium salt; HEK, human embryonic kidney; HSH, hypomagnesemia with secondary hypocalcemia; MagNuM, Mg^{2+}-nucleotide-inhibited; MIC, Mg^{2+}-inhibited cation; NCC, NaCl co-transporter; $NMDG^+$, *N*-methyl-D-glucosamine; RR, ruthenium red; TRP, transient receptor potential.

(HEK-293) cells and characterized using patch-clamp analysis in combination with Magfura-2-based intracellular Mg^{2+} measurements. Taken together, this study indicates that TRPM6 is a Mg^{2+}-permeable channel localized to the apical domain of the distal convoluted tubule and the brush-border membrane of the absorptive cells in duodenum, the main sites of transepithelial Mg^{2+} transport. The absence of the TRPM6-dependent Mg^{2+} influx pathway in patients with HSH provides a straightforward explanation for the severe hypomagnesemia.

EXPERIMENTAL PROCEDURES

Immunohistochemistry—Antiserum against TRPM6 was obtained by immunization of guinea pigs with a peptide encoding the carboxyl-terminal 15 amino acids of mouse TRPM6 (NH_2-ERDKNRSSLED-HTRL-COOH) coupled to key hole limpet hemocyanin. Kidneys from C57Bl/6 mice were cut into pieces, placed in 1% (w/v) periodate-lysine-paraformaldehyde fixative for 2 h, incubated overnight in phosphate-buffered saline containing 15% (w/v) sucrose, and frozen in liquid nitrogen. Duodenum samples from C57Bl/6 mice were cut into pieces, rinsed with phosphate-buffered saline, and frozen immediately in liquid nitrogen. Subsequently, kidney and duodenum samples were cut into 5–7-μm sections and used for different staining procedures as described previously (6). The antibody against parvalbumin was purchased from Swant (Bellinzona, Switzerland), whereas the NaCl co-transporter (NCC) antibody was kindly donated by Dr. J. Loffing (Zurich, Switzerland) (7). All negative controls, including sections incubated with pre-immune serum and undergoing pre-absorption for 1 h with 10 μg/ml TRPM6-peptide or solely with conjugated secondary antibodies, were devoid of any staining. Photographs were taken with a Bio-Rad MRC 1000 confocal laser-scanning microscope.

Electrophysiology, Intracellular Mg^{2+} Measurements, and Mg^{2+} Uncaging—HEK-293 cells were grown in Dulbecco's modified Eagle's medium containing 10% (v/v) fetal calf serum, 2 mM L-glutamine, 2 units/ml penicillin, and 2 mg/ml streptomycin at 37 °C in a humidity-controlled incubator with 10% CO_2. They were transiently transfected with human TRPM6 in the pCINeo/IRES-GFP vector using previously described methods (8), and electrophysiological recordings were made between 16 and 36 h after transfection. Successfully transfected cells were identified by their green fluorescence when illuminated at 480 nm. Patch-clamp experiments were performed in the tight seal whole-cell configuration at room temperature (20–25 °C) using an EPC-9 patch-clamp amplifier and Pulse software (HEKA Electronics). Currents were digitized at 10 kHz and digitally filtered at 2.9 kHz. Unless noted otherwise, cells were held at 0 mV, and voltage ramps of 200 ms duration ranging from −150 to 100 mV were applied every 2 s. Current densities were obtained by normalizing the current amplitude to the cell membrane capacitance. The time course of current development was determined by measuring the current in at 80 and −80 mV. The standard pipette solution contained 150 mM NaCl, 10 mM EDTA, and 10 HEPES mM, pH 7.2. Where indicated, NaCl was equimolarly substituted by NMDG-Cl. In some experiments, the EDTA was omitted, and 0.1 mM EGTA was added. The extracellular solutions contained 150 mM NaCl and 10 mM HEPES, pH 7.4, supplemented with either 10 mM EDTA (divalent-free solutions) or the indicated concentrations of divalent cations. To measure the relative permeability of divalent cations, we used solutions containing 120 mM NMDG-Cl and 10 mM HEPES, pH 7.4, supplemented with 20 mM of the chloride salt of the respective divalent cations.

The pipette solution used for the intracellular Mg^{2+} measurements (*e.g.* Fig. 3*a*) contained 150 mM NaCl, 0.1 mM EGTA, 0.2 mM Magfura-2, and 10 mM HEPES, pH 7.2. To measure the intracellular Mg^{2+} concentration, the dye was excited with light alternated between 350 and 380 nm using a monochromator-based system (TILL Photonics, Planegg, Germany), and the fluorescence signal was measured using a photodiode. The ratio R of the fluorescent signal at both wavelengths was converted into intracellular Mg^{2+} concentration using the Grynkiewicz equation (9). *In vivo* calibration constants were obtained by measuring R in cells dialyzed with pipette solutions containing 0, 2, and 100 mM free Mg^{2+}.

The pipette solution used in the Mg^{2+} uncaging experiments contained 150 mM NaCl, 5 mM DM-nitrophen, 4.5 mM $MgCl_2$, 1 mM Magfura-2, and 10 mM HEPES, pH 7.2. The estimated free Mg^{2+} concentration of this solution is 0.05 mM. Stepwise increases in intracellular Mg^{2+} were obtained by applying short flashes of UV light from a xenon arc flash lamp (Rapp OptoElectronics, Hamburg, Germany). We also performed experiments using a similar DM-nitrophen-containing pipette solution devoid of Mg^{2+}. Under these conditions, UV flashes had no significant effect on the whole-cell currents in TRPM6-expressing cells, thereby excluding direct effects of UV light or photolysis products of DM-nitrophen.

Data Analysis—Data analysis and display was done using Microcal Origin software, version 7.0 (OriginLab Corporation). Group data are presented as mean ± S.E. Student's t test and one-way analysis of variance (ANOVA) were used for statistical comparisons between means.

RESULTS AND DISCUSSION

The recent finding that the TRPM6 messenger is found in the kidney and small intestine (3, 2), prompted us to determine the (sub)cellular localization of the TRPM6 protein in these organs. Using antiserum raised against the last 15 amino acids of the mouse TRPM6 carboxyl-terminus (NH_2-ERDKNRSSLE-DHTRL-COOH), immunopositive staining was observed in the superficial cortex of the mouse kidney, whereas the outer and inner medulla were negative. Importantly, TRPM6 was predominantly localized to the apical membrane of the immunopositive tubules (Fig. 1*a*). Next, co-stainings were performed combining the antisera against TRPM6 and the thiazide-sensitive NCC, which is a specific marker for DCT, the main site of active transcellular Mg^{2+} reabsorption along the nephron (10). A complete co-localization of TRPM6 and NCC was observed in mouse kidney, as illustrated in Fig. 1*a*. The segmental distribution of TRPM6 was compared with that of parvalbumin and calbindin-D_{28K}, two cytosolic proteins that can act as endogenous Ca^{2+} and Mg^{2+} buffers (11). TRPM6 co-localized with parvalbumin in the proximal part of DCT (DCT1; Fig. 1*b*) and with calbindin-D_{28K} in the distal part of DCT (DCT2; Fig. 1*c*). Expression of calbindin-D_{28K} extended to TRPM6-negative cells in the connecting tubule and the cortical collecting duct (Fig. 1*c*). These results demonstrate that TRPM6 expression is restricted to DCT, where it is localized along the apical membrane (Fig. 1*d*). Interestingly, Schlingmann *et al.* reported the presence of TRPM6 mRNA in the proximal tubule (2). In the present study we did not, however, detect TRPM6 protein expression in this segment. Because TRPM6 mRNA was detected in the previous study by PCR using microdissected tubules, it is possible that small impurities of the dissected segments have been sufficient to yield a weak PCR band. In small intestine, TRPM6 was abundantly present in brush-border membranes of duodenum (Fig. 1*e*). Absorptive epithelial cells in the villi stained intensively for TRPM6. No staining was observed when duodenum sections were incubated with pre-immune antiserum (Fig. 1*e*, *right*).

For electrophysiological analysis of TRPM6, HEK-293 cells were transiently transfected with a vector containing the coding sequence for human TRPM6 (GenBank™ accession number NM_017662). Transfected cells perfused with a NaCl-based extracellular solution containing 1 mM $CaCl_2$ exhibited characteristic outwardly rectifying currents immediately upon establishment of the whole-cell configuration (Fig. 2, *a* and *c*). When dialyzed with a divalent-free internal solution containing 10 mM EDTA, the amplitude of these outwardly rectifying currents rapidly increased to reach a plateau level within 100–200 s (Fig. 2*a*). These outwardly rectifying currents showed little or no time dependence during voltage steps to different potentials (Fig. 2*d*). In agreement with previous reports (12, 13), we also observed outwardly rectifying currents in non-transfected HEK-293 cells dialyzed with a Mg^{2+}-free internal solution. However, when compared with TRPM6-expressing cells, these currents were undetectable immediately upon establishment of the whole-cell configuration, developed over a longer time period, and reached maximal amplitudes that were ~10 times smaller (Fig. 2*b*). HEK-293 cells transfected with two of the TRPM6 mutants identified in HSH patients ($TRPM6^{S590X}$ and

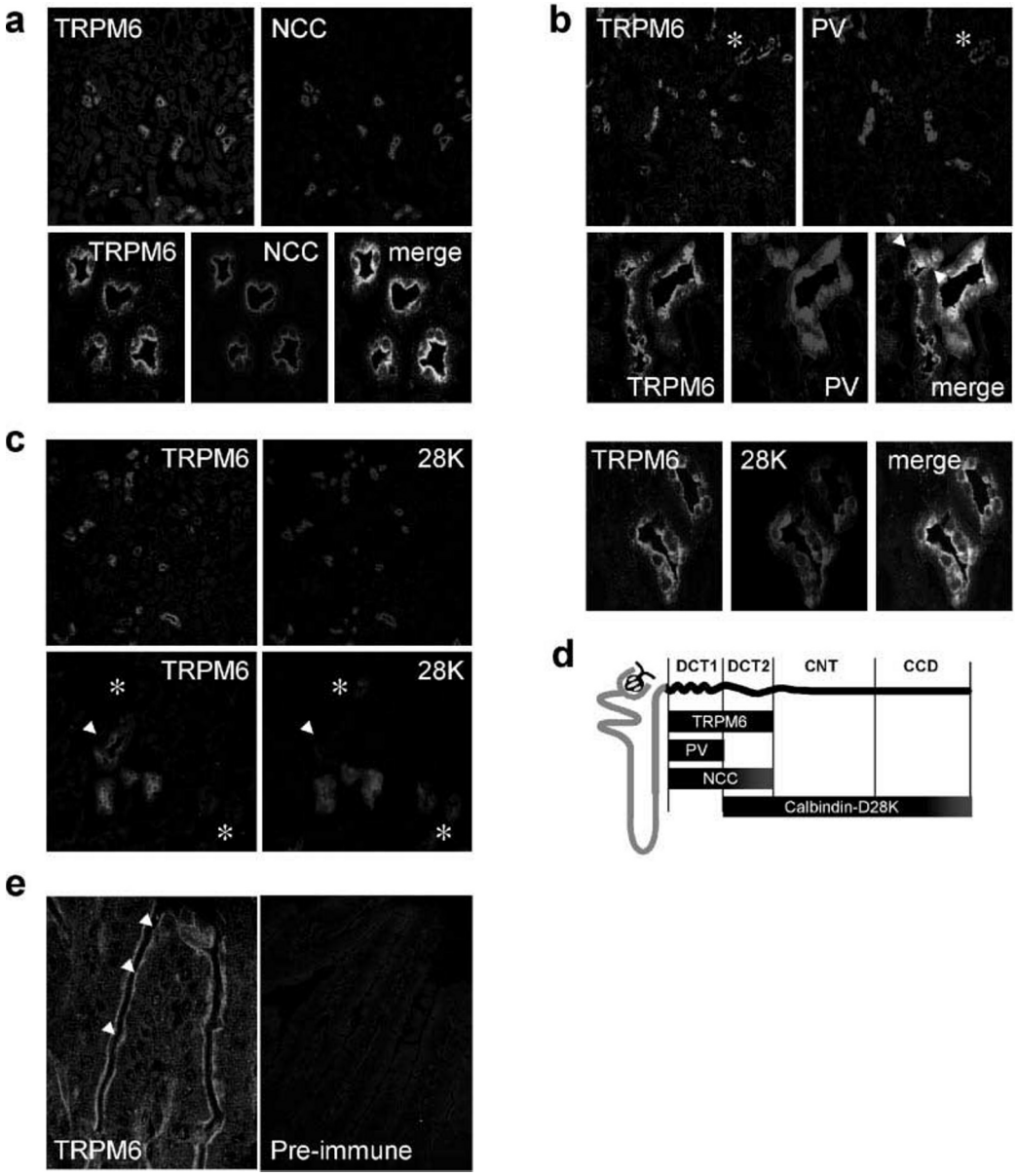

FIG. 1. **Distribution of TRPM6 along the nephron.** *a–c*, double immunofluorescence staining of mouse kidney cortex sections showing immunopositive staining for TRPM6 and NCC (*a*), TRPM6 and parvalbumin (*b*), and TRPM6 and calbindin-D_{28K} (*28K*) (*c*). The *asterisks* indicate DCT cells positive for calbindin-D_{28K} (*c*) and negative for parvalbumin (*b*) but positive for TRPM6, whereas the *arrowheads* mark DCT cells positive for TRPM6 but negative for parvalbumin (*b*) and calbindin-D_{28K} (*c*). *d*, schematic overview of the expression patterns of TRPM6, NCC, calbindin-D_{28K}, and parvalbumin (*PV*) along the nephron. *DCT1*, early part of DCT; *DCT2*, late part of DCT; *CNT*, connecting tubule; *CCD*, cortical collecting duct. *e*, immunofluorescence staining of TRPM6 in mouse duodenum (*left*). The *arrowheads* indicate the localization of the TRPM6 protein in the absorptive cells along the brush-border membrane of the villi. Sections incubated with the pre-immune antiserum did not show any staining, indicating the specificity of the antiserum.

$TRPM6^{Arg\text{-}736\ fs\ X\text{-}737}$, in which fs stands for frameshift and *X* is a stopcodon) displayed currents with similar amplitude and activation kinetics as non-transfected cells (Fig. 2, *a* and *b*), indicating that these mutant proteins are non-functional. Note that all mutations found in HSH patients code for truncated proteins that lack all six transmembrane domains as well as the carboxyl-terminal α-kinase domain (2, 3).

We next investigated the ionic nature of the TRPM6-induced currents. Using NaCl-based extracellular solutions containing low millimolar concentrations of $CaCl_2$ and/or $MgCl_2$, the outwardly rectifying TRPM6-induced currents reversed close to 0 mV (*e.g.* Fig. 2, *c* and *e*). Substitution of extracellular Cl^- by aspartate did not alter the reversal potential or amplitude of the outward currents (data not shown), excluding a significant contribution of Cl^- fluxes to the observed currents. Likewise, substitution of extracellular Na^+ by the large cation *N*-methyl-D-glucosamine ($NMDG^+$) did not change the shape of the current-voltage relation or the inward current amplitude; with both Mg^{2+} and Ca^{2+} at 2 mM in the extracellular solution, the inward current density at −80 mV was −13.6 ± 2.2 pA/pF and −13.7 ± 2.3 pA/pF ($n = 4$) in the presence of 150 mM Na^+ and $NMDG^+$, respectively. These results indicate that the inward current is almost exclusively carried by Mg^{2+} and/or Ca^{2+}. However, large inward currents were observed upon removal of all extracellular divalent cations, yielding slightly inwardly rectifying currents that reversed close to 0 mV with identical NaCl-based solutions on either side of the membrane (Fig. 2*e*). Subsequent substitution of extracellular Na^+ by $NMDG^+$ virtually abolished inward currents, shifting the reversal potential to voltages more negative than −50 mV (Fig. 2*e*). Thus, in the absence of divalent cations, the TRPM6-induced channel becomes highly permeable to Na^+. Outward currents were

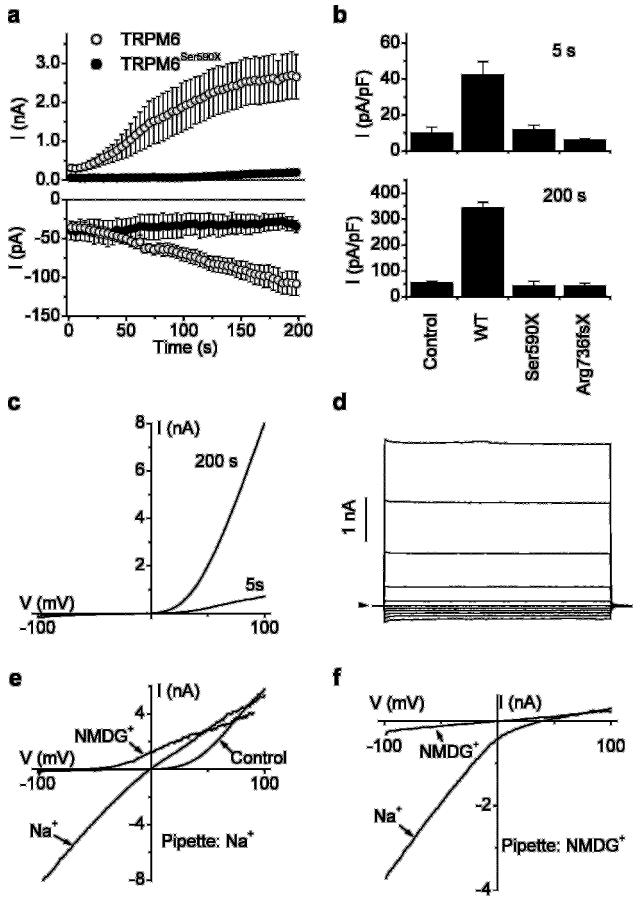

FIG. 2. **Functional expression of TRPM6 as a cation channel.** *a*, average time course of the development inward and outward currents at 80 and −80 mV in HEK-293 cells expressing wild-type TRPM6 or TRPM6^{S590X} (*TRPM6^{Ser590X}*) upon dialysis with the standard pipette solution. Extracellular solution contained 1 mM Ca^{2+} and no Mg^{2+}. *b*, average current densities at 80 mV measured 5 s (*top*) or 200 s (*bottom*) after whole-cell establishment in non-transfected HEK-cells (n = 15) and cells expressing wild-type TRPM6 (n = 42), TRPM6^{S590X} (*Ser590X*) (n = 6) or TRPM6$^{Arg\text{-}736\ fs\ X\text{-}737}$ (*Arg736fsX*; in which fs stands for frameshift and X is a stop codon) (n = 7). *c*, current-voltage relations from a TRPM6-transfected cell obtained under experimental conditions as in *panel a*, measured at the indicated times after whole-cell establishment. *d*, currents measured in a TRPM6-expressing cells during 100-ms steps to potentials ranging from −100 to 100 mV, 20 mV spaced. *e*, current-voltage relations obtained after maximal current activation using an extracellular solution containing 2 mM $MgCl_2$ and 2 mM $CaCl_2$ (*Control*) and, after superfusion, with divalent-free solution containing Na^+ or $NMDG^+$ as the sole extracellular cation. *f*, current-voltage relations obtained in divalent-free conditions with Na^+ or $NMDG^+$ as the sole extracellular cation and $NMDG^+$ as the sole intracellular cation.

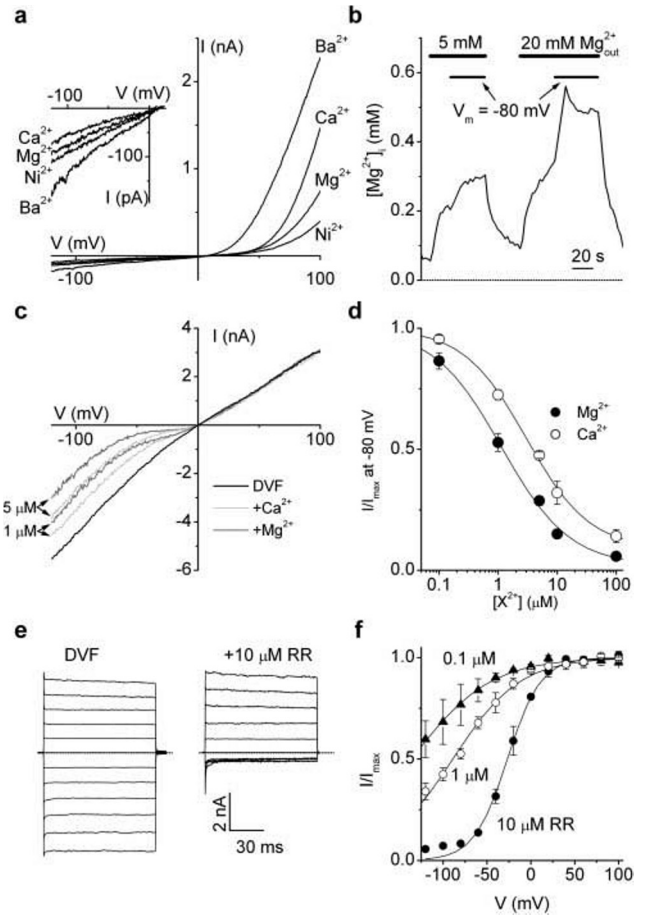

FIG. 3. **Divalent permeation and block of the TRPM6-induced channel.** *a*, current-voltage relations obtained with extracellular solutions containing 120 mM NMDG-Cl and 20 mM of the chloride salt of the indicated divalent cations. The *inset* represents an expanded view of the inward currents. *b*, ratiometric measurement of intracellular Mg^{2+} with Magfura-2 in a TRPM6-expressing cell. The cell was held at 0 mV, and voltage-ramps from −150 to 100 mV were applied every 2 s. When indicated, the holding potential was changed to −80 mV. Similar changes in intracellular Mg^{2+} were obtained in six TRPM6-expressing cells. Changes in intracellular Mg^{2+} were undetectable on this time scale in non-transfected cells (n = 4). *c*, current-voltage relations obtained in divalent-free (*DVF*) solution and in the presence of 1 and 5 μM of Ca^{2+} or Mg^{2+}. *d*, dose-response curves for the inhibition of inward Na^+ current at −80 mV by Ca^{2+} and Mg^{2+}. *e*, currents measured in divalent-free (*DVF*) solution during 100-ms steps to potentials ranging from −100 to 100 mV before and during extracellular application of 10 μM ruthenium red. *f*, voltage dependence of the block of the TRPM6-induced current in divalent-free solution for three different ruthenium red concentrations.

strongly reduced when $NMDG^+$ was the sole cation in the intracellular solution, indicating that the large outward currents observed with the NaCl-based intracellular solutions are mainly carried by Na^+ (Fig. 2*f*). Thus, the outwardly rectifying current-voltage profile of the TRPM6-induced current measured with physiological concentrations of extracellular divalent cations reflects the small inward flux of divalent cations and the large outward flux of monovalent cations.

Given that TRPM6 is expressed in Mg^{2+}-absorbing epithelia and that mutations in the *TRPM6* gene cause HSH, we further tested the permeability of the TRPM6-induced channel to Mg^{2+} and other divalent cations. Significant inward currents were measured with all tested divalent cations, each acting as the sole charge carrier in the extracellular solution (Fig. 3*a*). At a concentration of 20 mM, the permeation rank order determined from the inward current amplitude at −80 mV was $Ba^{2+} \geq Ni^{2+} > Mg^{2+} > Ca^{2+}$ (Fig. 3*a*, *inset*). When normalized to the inward current amplitude in 20 mM Ca^{2+}, we obtained relative values of 2.02 ± 0.18, 1.81 ± 0.22, and 1.33 ± 0.09 for Ba^{2+}, Ni^{2+}, and Mg^{2+}, respectively (n = 4–7). The divalent cations had a differential blocking effect on the outward currents, and the rank order of blocking efficiency was $Ni^{2+} > Mg^{2+} > Ca^{2+} > Ba^{2+}$ (Fig. 3*a*).

We also estimated permeability ratios (P_X/P_{Na}) based on the reversal potentials (E_{rev}) measured with the respective divalent cations (each 20 mM) in the extracellular solution and 150 mM intracellular Na^+. This procedure yielded a different permeation sequence (respective P_X/P_{Na} values in parentheses), namely Ni^{2+} (9.2 ± 0.3) > Mg^{2+} (9.0 ± 0.4) > Ca^{2+} (6.9 ± 0.3) > Ba^{2+} (6.2 ± 0.2). It is, for two reasons, questionable whether these P_X/P_{Na} values adequately describe the permeability properties of TRPM6. First, the slope of the current-voltage relation is very shallow around E_{rev} in the presence of

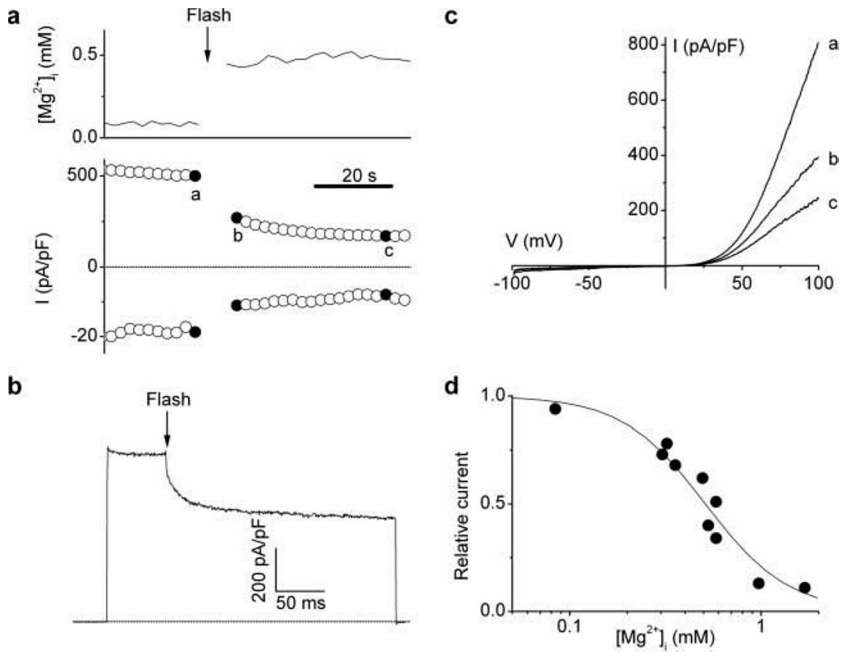

FIG. 4. **Rapid inhibition of the TRPM6-induced cation channel upon flash photolysis of caged Mg^{2+}.** *a*, simultaneous recording of intracellular Mg^{2+} (*top*) and the whole-cell current at 80 and −80 mV (*bottom*) before and after flash photolysis (*arrow*) of DM-nitrophen in a TRPM6-expressing cell. *b*, outward current during a 100-ms step to 100 mV, which was recorded during the gap in the recording shown in *panel a*, showing the rapid current inhibition after the flash. *c*, current-voltage relations obtained at the time points indicated in *panel a*. *d*, dose-response curve showing the inhibition of the TRPM6-induced currents by flash-induced increases in intracellular Mg^{2+} to different levels. Outward current amplitude was measured 45 s after the flash and normalized to the current amplitude before the flash. The intracellular Mg^{2+} concentration before the flash was ≤ 0.1 mM.

extracellular divalent cations. Exact measurements of E_{rev} are therefore difficult and error prone, because small changes in background current can have significant effects on E_{rev}. Second, the calculation of P_X/P_{Na} from E_{rev} is based on the Goldman-Hodgkin-Katz equations, which assume that ions permeate independently and that the electric field in the membrane is constant (14, 12). However, the outward rectification of the TRPM6-induced current is much stronger than predicted by these equations, which makes the validity of these assumptions highly questionable.

To further substantiate the Mg^{2+} permeability of the TRPM6-induced channel, we measured changes in the intracellular Mg^{2+} concentration directly using the Mg^{2+}-sensitive ratiometric dye Magfura-2. In these experiments, cells were dialyzed with a Magfura-2-containing pipette solution devoid of Mg^{2+} and EDTA (see "Experimental Procedures"), which resulted in basal intracellular Mg^{2+} concentrations between 0.05 and 0.1 mM (Fig. 3*b*). The addition of 5 mM Mg^{2+} to the extracellular solution, which contained 2 mM Ca^{2+} during the entire course of the experiment, resulted in a significant increase of the intracellular Mg^{2+} concentration in TRPM6-expressing cells (Fig. 3*b*). Intracellular Mg^{2+} was increased further with higher extracellular Mg^{2+} concentrations or when the plasma membrane was hyperpolarized to −80 mV (Fig. 3*b*), consistent with Mg^{2+} influx through the TRPM6-induced channel.

It is generally assumed that the luminal concentration of free Mg^{2+} in the Mg^{2+}-absorbing part of the nephron is in the range of 0.2–0.7 mM (1). To preferentially conduct Mg^{2+} in the presence of Ca^{2+}, which is present at a concentration of ~1 mM, the apical Mg^{2+} influx pathway should exhibit a higher affinity for Mg^{2+} than for Ca^{2+}. As a first approach to investigating whether the TRPM6-induced current satisfies this requirement, we compared the sensitivity of monovalent TRPM6-induced currents to Mg^{2+} and Ca^{2+}. As shown in Fig. 3*c*, inward Na^+ currents were blocked in a voltage-dependent manner by low micromolar concentrations of both Mg^{2+} and Ca^{2+}. However, Mg^{2+} blocked the inward currents at lower concentrations than Ca^{2+} (Fig. 3, *c* and *d*). The dose-response curves for block of Na^+ current at −80 mV yielded K_D values of 1.1 and 4.8 μM and Hill coefficients of 0.85 and 0.83 for Mg^{2+} and Ca^{2+}, respectively. The most straightforward explanation of the difference in K_D values between Mg^{2+} and Ca^{2+} is that Mg^{2+} binds with a higher affinity to a binding site in the channel pore. Alternatively, the inhibitory effect of divalent cations on the permeation of monovalent cations might be due to a regulatory divalent cation binding site outside the pore, but this is highly unlikely given the strong voltage dependence of the block by Mg^{2+} and Ca^{2+}. Thus, although the relative contribution of Mg^{2+} and Ca^{2+} to the inward current under physiological conditions is hard to estimate and expected to vary with changes in their respective extracellular concentrations, these data indicate that the pore of the TRPM6-induced channel has a higher affinity for Mg^{2+} than for Ca^{2+}. This contrasts with all known Ca^{2+}-selective channels (15, 14), including members of the TRP superfamily (16), which generally display a 10–1000 times lower affinity for Mg^{2+} than for Ca^{2+}.

Monovalent currents were highly sensitive to ruthenium red (RR), a potent blocker of several members of the TRPV family (17, 18). As illustrated in Fig. 3*e*, 10 μM RR caused a strong inhibition of inward monovalent currents while leaving outward currents unaltered. Fig. 3*f* summarizes the voltage and concentration dependence of the block of monovalent currents by RR. The RR concentration for half-maximal current inhibition increased from ~100 nM at −120 mV to >10 μM at potentials more positive than −20 mV. Such voltage dependence is generally interpreted as a direct block of the channel pore within the transmembrane electrical field. Interestingly, we found that inward currents carried by 10 mM Mg^{2+} were significantly less sensitive to inhibition by RR (40 ± 7% block at −80 mV with 10 μM RR; $n = 4$), suggesting that Mg^{2+} and RR compete with each other for one or more binding sites within the channel pore. Alternatively, Mg^{2+} might have an allosteric effect on the RR binding site.

TRPM6-induced currents increased significantly upon dialysis with Mg^{2+}-free intracellular solutions (*e.g.* Fig. 2*a*), indicating that intracellular Mg^{2+} has an inhibitory effect on TRPM6 activity. To test the effect of intracellular Mg^{2+} in a more direct manner, we performed experiments in which the intracellular Mg^{2+} concentration was directly altered in a spatially uniform manner using flash photolysis of the photolabile Mg^{2+}chelator DM-nitrophen (19). Fig. 4*a* shows an experiment in which a TRPM6-expressing cell was intracellularly dialyzed with a pipette solution containing 5 mM DM-nitrophen 90% saturated with Mg^{2+} as well as the Mg^{2+}-sensitive dye Mag-

fura-2. After maximal activation of the current, a brief flash (~1 ms) of UV light was applied to the cell and the tip of the patch pipette, which resulted in a stepwise increase of the intracellular Mg^{2+} concentration from < 0.1 mM to ~0.5 mM (Fig. 4*a*, *top*). As a result of the increased intracellular Mg^{2+}, the TRPM6-induced current was significantly reduced, both at positive and negative potentials (Fig. 4a, *bottom*). We observed two temporal phases in the Mg^{2+}-induced current reduction. As shown in Fig. 4*b*, the outward current at +100 mV rapidly decreased after the flash-induced increase in intracellular Mg^{2+} with an initial time constant of 24 ± 5 ms at 0.51 ± 0.07 mM Mg^{2+} ($n = 5$). Thereafter, a second, slower phase of inhibition was observed, which was complete in ~ 30–40 s (time constant 21 ± 3 s; $n = 5$). Fig. 4*c* compares current-voltage relations obtained just before and, respectively, 5 and 45 s after the flash, illustrating that the inhibitory effect of intracellular Mg^{2+} displays little or no voltage dependence. Fig. 4*d* displays the relative current 45 s after the flash in the function of the post-flash Mg^{2+} concentration. The *solid line* (Fig. 4*d*) represents a dose-response curve fitted to the data, which yielded an apparent K_D of 0.51 mM and a Hill coefficient of 2.1.

Most of our experiments were performed with a pipette solution containing 10 mM EDTA, which causes slow passive depletion of the intracellular Ca^{2+} stores. Given that several members of the TRP family have been shown to be store-dependent (4), we reasoned that part of the current activation after establishment of the whole-cell configuration might reflect store dependence of TRPM6. To test this possibility, we measured whole-cell currents using a Mg^{2+}-free pipette solution containing 0.1 mM EGTA as the sole Ca^{2+} buffer, which is not sufficient to cause significant store depletion within the time course of our experiments. Under this condition, TRPM6-expressing cells still developed robust outwardly rectifying currents, and the average current density (319 ± 58 pA/pF; $n = 8$) was not different from that of cells dialyzed with the standard solution containing 10 mM EDTA (341 ± 24 pA/pF; $n = 42$; see Fig. 1*b*). Moreover, depletion of the intracellular stores by extracellular application of the sarcoendoplasmic reticulum Ca^{2+}-ATPase inhibitor 2,5-di-*t*-butyl-1,4-benzohydroquinone (20 μM) or the Ca^{2+} ionophore ionomycin (2 μM) did not alter the amplitude of the TRPM6-induced currents measured with 0.1 mM EGTA in the pipette solution ($n = 3$ for each drug; data not shown). From this we conclude that the activity of TRPM6 does not critically depend on the filling state of the intracellular Ca^{2+} stores.

The TRPM6-induced currents are highly reminiscent of the currents induced by overexpression of TRPM7 in HEK-293 or Chinese hamster ovary cells (5, 13) as well as to the outwardly rectifying currents regulated by intracellular Mg^{2+} and/or Mg^{2+}-nucleotides that are present in cell types (including HEK-293 cells) that endogenously express TRPM7 and have been termed MagNuM (for Mg^{2+}-nucleotide-inhibited) or MIC (Mg^{2+}-inhibited cation) currents (13, 20–22). The list of similarities between the TRPM6-induced currents and the TRPM7, MagNuM, or MIC currents includes the outwardly rectifying current-voltage relation, the lack of voltage dependence, and the sensitivity to intracellular Mg^{2+}. This raises the important question of whether the currents described in this study are mediated by TRPM6 itself or rather represent the activity of the endogenously expressed TRPM7. However, this possibility is rather unlikely for the following reasons. First, current amplitudes in TRPM6-expressing cells were ~10 times larger than in non-transfected cells, and developed much faster when intracellular Mg^{2+} was buffered. Second, no significant increase in outwardly rectifying currents was observed upon overexpression of two HSH-causing TRPM6 mutants. Finally, the average current density in TRPM6-expressing HEK-293 cells measured in this study was of the same order of magnitude and even larger than those reported for HEK-293 or CHO cells overexpressing TRPM7 under comparable experimental conditions (5, 13, 20–23). Thus, the most straightforward explanation of our findings is that TRPM6 forms all or a major part of a Mg^{2+}-permeable cation channel regulated by intracellular Mg^{2+}.

TRPM6 and TRPM7 have an overall amino acid sequence identity of 52%, which increases to >80% in the region between the fifth and sixth transmembrane region where the pore-forming loop is presumably located. Moreover, both TRPM6 and TRPM7 have a carboxyl-terminal region with sequence similarities to the atypical α-kinase family. Given this high degree of homology, it cannot be excluded that TRPM6 and TRPM7 are able to form heterotetrameric channels, similar to what has been described for TRPV5/TRPV6 (24) and TRPC1/TRPC5 (25). However, the 10-fold larger current amplitude in the TRPM6-expressing cells compared with non-transfected HEK-293 cells indicates that the majority of the channels are actually TRPM6 homotetramers. As a consequence of our findings, some caution is warranted when equating endogenous MagNuM (MIC) currents to TRPM7, as TRPM6 or putative TRPM6-TRPM7 heteromultimers might underlie these currents in some cell types.

In conclusion, we have demonstrated that TRPM6 confines a Mg^{2+}-permeable channel that is specifically localized to the apical membrane of Mg^{2+}-reabsorbing tubules in the kidney and the brush-border membrane of the Mg^{2+} absorptive cells in the duodenum. The tight regulation of the TRPM6-induced current by intracellular Mg^{2+} provides a feedback mechanism on Mg^{2+} influx and implies that intracellular Mg^{2+} buffering and Mg^{2+} extrusion mechanisms strongly impact on channel functioning. Parvalbumin and calbindin-D_{28K}, which, as shown in this work, are co-expressed with TRPM6, might function as intracellular Mg^{2+} chelators in the DCT, although further studies are needed to substantiate this. To our knowledge, TRPM6 represents the first molecularly identified and functionally characterized component of active Mg^{2+} (re)absorption. The absence of the TRPM6-dependent Mg^{2+} influx pathway in kidney and the small intestine provides a straightforward explanation for the severe hypomagnesemia observed in HSH patients.

Acknowledgments—We thank Drs. A. Ryazanov for kindly providing a partial cDNA clone encoding human TRPM6 (GenBank™ accession number AF350881), J. Loffing for the antibody against NCC, J. Prenen and A. Janssens for technical assistance, and K. Talavera, G. Owsianik, and C. van Os for stimulating discussions.

REFERENCES

1. Dai, L. J., Ritchie, G., Kerstan, D., Kang, H. S., Cole, D. E., and Quamme, G. A. (2001) *Physiol. Rev.* **81,** 51–84
2. Schlingmann, K. P., Weber, S., Peters, M., Niemann Nejsum, L., Vitzthum, H., Klingel, K., Kratz, M., Haddad, E., Ristoff, E., Dinour, D., Syrrou, M., Nielsen, S., Sassen, M., Waldegger, S., Seyberth, H. W., and Konrad, M. (2002) *Nat. Genet.* **31,** 166–170
3. Walder, R. Y., Landau, D., Meyer, P., Shalev, H., Tsolia, M., Borochowitz, Z., Boettger, M. B., Beck, G. E., Englehardt, R. K., Carmi, R., and Sheffield, V. C. (2002) *Nat. Genet.* **31,** 171–174
4. Montell, C., Birnbaumer, L., and Flockerzi, V. (2002) *Cell* **108,** 595–598
5. Runnels, L. W., Yue, L., and Clapham, D. E. (2001) *Science* **291,** 1043–1047
6. Hoenderop, J. G., Hartog, A., Stuiver, M., Doucet, A., Willems, P. H., and Bindels, R. J. (2000) *J. Am. Soc. Nephrol.* **11,** 1171–1178
7. Nijenhuis, T., Hoenderop, J. G., Loffing, J., van der Kemp, A. W., Van Os, C., and Bindels, R. J. (2003) *Kidney Int.* **64,** 555–564
8. Trouet, D., Nilius, B., Voets, T., Droogmans, G., and Eggermont, J. (1997) *Pfluegers Arch. Eur. J. Physiol.* **434,** 632–638
9. Grynkiewicz, G., Poenie, M., and Tsien, R. Y. (1985) *J. Biol. Chem.* **260,** 3440–3450
10. Obermuller, N., Bernstein, P., Velazquez, H., Reilly, R., Moser, D., Ellison, D. H., and Bachmann, S. (1995) *Am. J. Physiol.* **269,** F900–F910
11. Yang, W., Lee, H. W., Hellinga, H., and Yang, J. J. (2002) *Proteins* **47,** 344–356
12. Monteilh-Zoller, M. K., Hermosura, M. C., Nadler, M. J., Scharenberg, A. M., Penner, R., and Fleig, A. (2003) *J. Gen. Physiol.* **121,** 49–60

13. Nadler, M. J., Hermosura, M. C., Inabe, K., Perraud, A. L., Zhu, Q., Stokes, A. J., Kurosaki, T., Kinet, J. P., Penner, R., Scharenberg, A. M., and Fleig, A. (2001) *Nature* **411,** 590–595
14. Hille, B. (2001) *Ion Channels of Excitable Membranes,* Sinauer Associates, Sunderland, MA
15. Hess, P., and Tsien, R. W. (1984) *Nature* **309,** 453–456
16. Hoenderop, J. G., Vennekens, R., Muller, D., Prenen, J., Droogmans, G., Bindels, R. J., and Nilius, B. (2001) *J. Physiol.* **537,** 747–761
17. Caterina, M. J., Schumacher, M. A., Tominaga, M., Rosen, T. A., Levine, J. D., and Julius, D. (1997) *Nature* **389,** 816–824
18. Nilius, B., Prenen, J., Vennekens, R., Hoenderop, J. G., Bindels, R. J., and Droogmans, G. (2001) *Br. J. Pharmacol.* **134,** 453–462
19. Kaplan, J. H., and Ellis-Davies, G. C. (1988) *Proc. Natl. Acad. Sci. U. S. A.* **85,** 6571–6575
20. Prakriya, M., and Lewis, R. S. (2002) *J. Gen. Physiol.* **119,** 487–507
21. Hermosura, M. C., Monteilh-Zoller, M. K., Scharenberg, A. M., Penner, R., and Fleig, A. (2002) *J. Physiol.* **539,** 445–458
22. Kozak, J. A., Kerschbaum, H. H., and Cahalan, M. D. (2002) *J. Gen. Physiol.* **120,** 221–235
23. Runnels, L. W., Yue, L., and Clapham, D. E. (2002) *Nat. Cell Biol.* **4,** 329–336
24. Hoenderop, J. G., Voets, T., Hoefs, S., Weidema, A. F., Prenen, J., Nilius, B., and Bindels, R. J. (2003) *EMBO J.* **22,** 776–785
25. Strubing, C., Krapivinsky, G., Krapivinsky, L., and Clapham, D. E. (2001) *Neuron* **29,** 645–655